A FLEXIBLE QUADRANGULAR MESH TILING A CYLINDER OF REVOLUTION

Hellmuth STACHEL
Vienna University of Technology, Austria

ABSTRACT: Due to A. Kokotsakis a quad mesh consisting of congruent convex quadrangles of a planar tessellation is flexible. This means, when the quadrangles are seen as rigid bodies and only the dihedral angles along internal edges can vary, the mesh admits incongruent realizations in 3-space, so-called flexions. It has recently be proved by the author that at each nontrivial flexion all vertices lie on a cylinder of revolution. The complete quad mesh can be obtained from a pair of neighbouring quadrangles by applying products of two coaxial helical displacements. These displacements convert at the initial flat pose into translations generating the flat tessellation.
The goal of this paper is to give sufficient conditions for the initial convex quadrangle and the bending angles such that the corresponding particular flexion forms a tiling on a cylinder, i.e., after bending around a cylinder the two boundaries fit precisely together.

Keywords: quad mesh, flexible polyhedra, Kokotsakis mesh, origami mechanisms, cylinder tiling

1. INTRODUCTION

A *quadrangular mesh* ('quad mesh' by short) is a simply connected subset of a polyhedral surface consisting of planar quadrangles, edges and vertices in the Euclidean 3-space. The edges are either *internal* when they are shared by two faces, or they belong to the boundary of the mesh.

Let the quadrangles be rigid bodies; only the dihedral angles along internal edges can vary. A quad mesh is called *continuously flexible* when there is a one-parameter set of mutually incongruent realizations of this mesh in 3-space, so-called *flexions*. The continuous movement of the mesh is called a *self-motion*.

A complete classification of all continuously flexible quad meshes is still open (compare, e.g., [1]). Open is in particular the classification of the 3×3 quad meshes, the so-called *Kokotsakis meshes*, named after Antonios Kokotsakis [2]. In [3] a list of five flexible types is presented.

In the following we study the flexions of a very special example (cf. [2]) whose 3×3 submeshes are of type 5 according to the list mentioned above. The flat initial pose of this flexible quad mesh consists of the planar tessellation as displayed in Fig. 1.

2. TESSELLATION MESHES

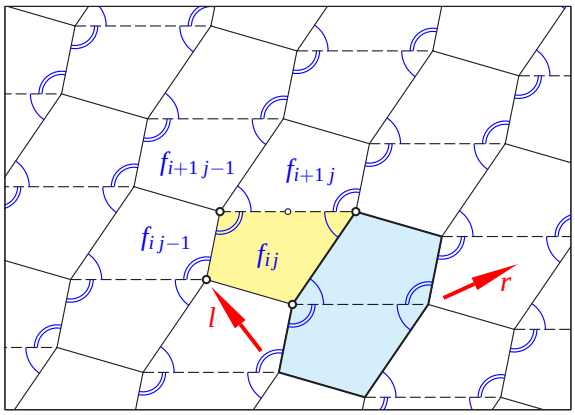

Figure 1: Kokotsakis' flexible tessellation.

The following continuously flexible quad mesh dates back to A. Kokotsakis [2, p. 647]. Its initial pose is flat and consists of congruent convex quadrangles of a planar tessellation.

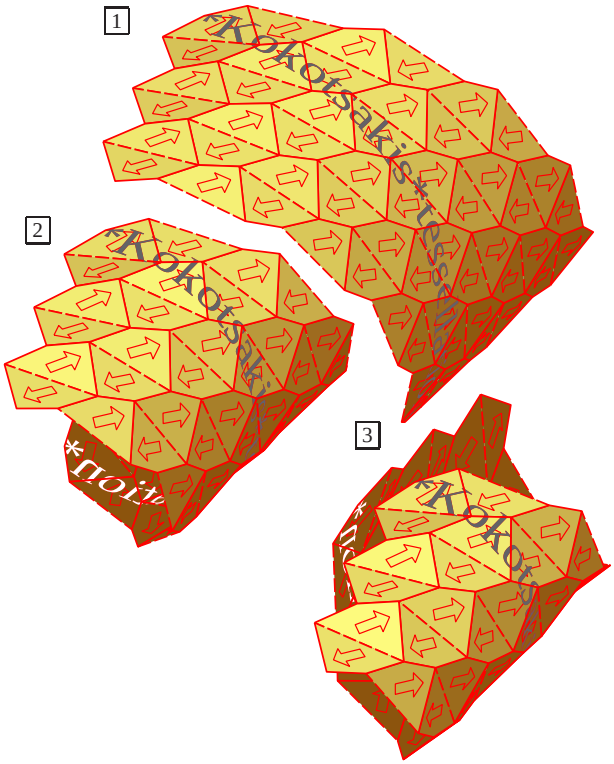

Figure 2: Flexions of a 9×6 tessellation mesh. Dashes indicate valley folds.

Any two quadrangles sharing an edge (like f_{ij} and $f_{i+1\,j}$ in Fig. 1) change place under a rotation through 180° (= *half-turn*) about the midpoint of the common edge. Such a pair of adjacent quadrangles forms a centrally symmetric hexagon (see blue shaded area in Fig. 1), and the complete tessellation can be generated by iterated translations of this hexagon. The arrows in Fig. 1 indicate the directions of these generating translations r and l.

We recall a theorem from [4, Thm. 6, p. 12] where the flexions obtainable by a continuous one-parameter self-motion are characterized. Additional degrees of freedom of single faces on the boundary of the mesh were excluded by the request: Whenever the tessellation mesh includes three faces with a common vertex, then also the fourth face of this pyramid should be included.

Thus we obtain a rectangular grid of $m \times n$ quadrangles. There is a natural way to denote the quadrangles by f_{ij} with $1 \le i \le m$ and $1 \le j \le n$. This is what we call a $m \times n$ *tessellation mesh*:

$$\begin{array}{ccccc} f_{m1} & f_{m2} & f_{m3} & \cdots & f_{mn} \\ \vdots & \vdots & \vdots & & \vdots \\ f_{21} & f_{22} & f_{23} & \cdots & f_{2n} \\ f_{11} & f_{12} & f_{13} & \cdots & f_{1n} \end{array}$$

The sequences of edges between consecutive 'rows' $\{f_{ij} \,|\, j = 1,\ldots,n\}$ and $\{f_{i+1\,j} \,|\, j = 1,\ldots,n\}$, $1 \le i < m$, are called *horizontal folds*. Those between the 'columns' $\{f_{ij} \,|\, i = 1,\ldots,m\}$ and $\{f_{i\,j+1} \,|\, i = 1,\ldots,m\}$, $1 \le j < n$, form the *vertical folds* of the mesh.

When the basic quadrangle is a trapezoid, then in the flat pose the folds of one type are aligned. About each of these folds the mesh can be bended, independently from each other. We call these particular flexions *trivial*. However, the same mesh admits also nontrivial flexions (note Fig. 10), except the case with a basic parallelogram.

Theorem 1. [4] *Each $m \times n$ tessellation mesh with convex quadrangles is flexible. At each nontrivial flexion obtainable by a self-motion the vertices are located on a cylinder of revolution (Fig. 6). The images of two neighbouring quadrangles under iterated coaxial helical displacement r and l cover the complete mesh. The union of these two fundamental quadrangles is a line-symmetric hexagon.*

Here is a summary of the proof presented in [4]: We start with the four faces $f_{11}, f_{12}, f_{22}, f_{21}$ with vertex V_1 (blue shaded area in Fig. 3). These pairwise congruent faces of a 2×2 tessellation mesh form a four-sided pyramid. It is flexible, provided the fundamental quadrangle is convex. Otherwise, one interior angle of a face at V_1 is greater than the sum of the other three interior angles so that the pyramid admits only the flat realization.

Let a non-planar flexion of this pyramid be given (Fig. 4). For any pair (f_{11}, f_{12}), …, (f_{21}, f_{11}) of adjacent faces there is a respective

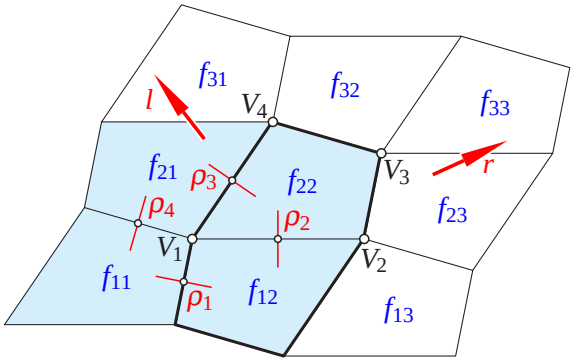

Figure 3: The complete flexion can be generated by applying iterated half-turns $\rho_1,\dots,\rho_4$ to an initial face f_{11}.

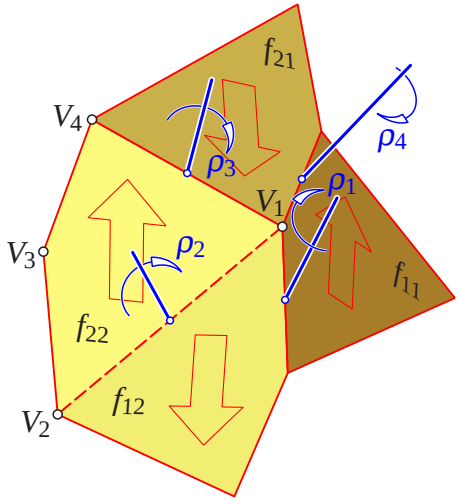

Figure 4: A flexion of a 2×2 tessellation mesh.

half-turn $\rho_1,\dots,\rho_4$ which swaps the two faces. So, e.g., $f_{12}=\rho_1(f_{11})$ and $f_{11}=\rho_1(f_{12})$. The axis of ρ_1 is perpendicular to the common edge of f_{11} and f_{12}, and it is located in the plane which bisects the dihedral angle between f_{11} and f_{12}.

After applying the four half-turns $\rho_1,\dots,\rho_4$ consecutively, the quadrangle f_{11} is mapped via f_{12}, f_{22}, and f_{21} onto itself. Hence the product $\rho_4\dots\rho_1$ equals the identity. (We indicate the composition of mappings by left multiplication.) Because of $\rho_i^{-1}=\rho_i$ for $i=1,\dots,4$ we obtain

$$\rho_2\rho_1=\rho_3\rho_4. \qquad (1)$$

Now we recall a standard result from the geometry in 3-space: The product of two half-turns about non-parallel axes a_1,a_2 is a helical displacement:

- its axis is the common perpendicular of a_1 and a_2;
- its angle of rotation is twice the angle made by a_1 and a_2;
- its length of translation is twice the distance between a_1 and a_2.

When the axes of ρ_1 and ρ_2 are parallel (compare Fig. 4) they are orthogonal to two adjacent edges of f_{12} and therefore orthogonal to the face f_{12}. As a consequence all four faces $f_{11},\dots,f_{21}$ are coplanar. Hence conversely, when our pyramid with apex V_1 is not flat, then the axes of neighbouring half-turns cannot be parallel. Their common perpendicular is unique. Therefore (1) implies that the axes of the four half-turns have a common perpendicular p.

Lemma 2. *At each non-flat flexion of a tessellation mesh the displacements $\rho_2\rho_1=\rho_3\rho_4$ and $\rho_4\rho_1=\rho_3\rho_2$ are helical motions with a common axis p. In the initial flat pose they convert into the generating translations r and l (see Fig. 1).*

Now we extend the flexion of the 2×2 tessellation mesh (shaded area in Fig. 3) step by step to the complete $m\times n$ mesh by adding congruent copies of the initial pyramid without restricting the flexibility:

The half-turn ρ_2 exchanges not only f_{12} with f_{22} but maps the pyramid with apex V_1 onto a congruent copy with apex V_2 sharing two faces with its preimage. We get $f_{13}=\rho_2(f_{21})$ and $f_{23}=\rho_2(f_{11})$. Analogously, ρ_3 generates a pyramid with apex V_4 which shares the two faces f_{22} and f_{21} with the initial pyramid, and $f_{31}=\rho_3(f_{12})$, $f_{32}=\rho_3(f_{11})$.

Finally there are two ways to generate a pyramid with apex V_3. Either, we transform ρ_1 by ρ_2 and apply $\rho_2\rho_1\rho_2$, which exchanges f_{22} with f_{23} and swaps V_2 and V_3. Or we proceed with

$\rho_3\rho_4\rho_3$, which exchanges f_{22} with f_{32} and swaps V_4 and V_3.

Thus we obtain mappings $(\rho_2\rho_1\rho_2)\rho_2 = \rho_2\rho_1$ and $(\rho_3\rho_4\rho_3)\rho_3 = \rho_3\rho_4$ with $V_1 \mapsto V_3$. Both displacements are equal by (1), and we notice

$$\begin{aligned}\rho_2\rho_1 = \rho_3\rho_4\colon\ & f_{11} \mapsto f_{22},\ f_{12} \mapsto f_{23},\\ & f_{22} \mapsto f_{33},\ f_{21} \mapsto f_{32}.\end{aligned} \tag{2}$$

Hence each flexion of the initial pyramid with apex V_1 is compatible with a flexion of the 3×3 tessellation mesh displayed in Fig. 3. It is proved in [4, Lemma 8] that this the only way to continue the given flexion of the 2×2 tessellation mesh, provided we restrict to flexions obtainable by a continuous self-motion from the initial flat pose.

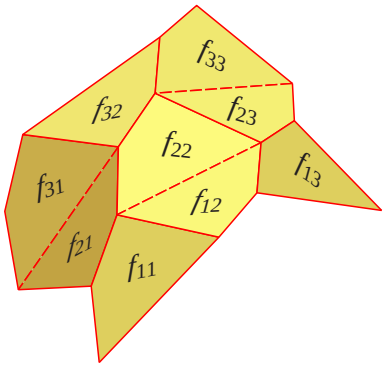

Figure 5: Flexion of a 3×3 tessellation mesh.

Next, we continue this flexion of the 3×3 mesh to the complete $m\times n$ tessellation mesh by proceeding 'column' by 'column' (see, e.g., Fig. 7) to the right and 'row' by 'row' upwards.

According to Lemma 2 the helical displacements $\rho_2\rho_1$ and $\rho_4\rho_1 = \rho_3\rho_2$ are the spatial analogues of the generating translations in the plane. $\rho_2\rho_1$ maps V_1 onto V_3, and $\rho_4\rho_1$ maps the pyramid with apex V_2 onto that with apex V_4; thus we have

$$\begin{aligned}\rho_4\rho_1 = \rho_3\rho_2\colon\ & f_{12} \mapsto f_{21},\ f_{13} \mapsto f_{22},\\ & f_{23} \mapsto f_{32},\ f_{22} \mapsto f_{31}.\end{aligned} \tag{3}$$

When f_{12} and f_{22} are glued together, we obtain a skew hexagon, one half of our initial pyramid with apex V_1 (see Fig. 3). The half-turn ρ_2

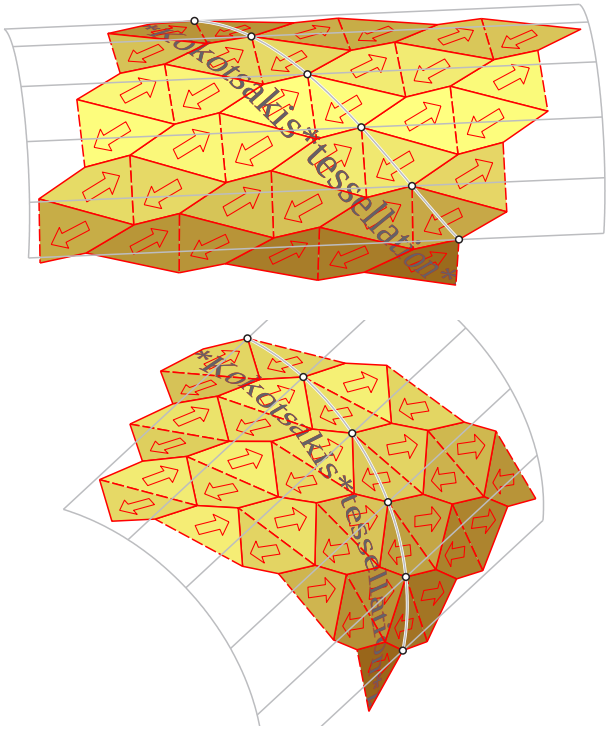

Figure 6: For each flexion of the first and second kind the vertices are placed on a cylinder of revolution; the marked points are located on a helical line. Again, dashes indicate valley folds.

maps this hexagon onto itself; hence it is line-symmetric. By (2) the helical displacement $\rho_2\rho_1$ maps this hexagon onto the compound of f_{23} and f_{33}. It is the spatial analogue of the translation r indicated in Fig. 1 by the red arrow pointing upwards to the right. The displacement $\rho_4\rho_1$ maps the compound of f_{12} and f_{22} onto f_{21} and f_{31}. When these two helical displacements act repeatedly on the line-symmetric hexagon, the complete flexion is obtained. We denote

$$\begin{aligned} r := \rho_2\rho_1 = \rho_3\rho_4\colon\ & V_1 \mapsto V_3,\\ l := \rho_4\rho_1 = \rho_3\rho_2\colon\ & V_2 \mapsto V_4.\end{aligned} \tag{4}$$

Coaxial helical displacements about p together with rotations and pure translations along p constitute a commutative group; hence $rl = lr$.

All vertices of the flexion arise from V_1 by displacements which keep the common perpendicular p of the half-turns' axes fixed. For example,

according to Fig. 3

$$V_2 = \rho_2(V_1),\ V_3 = r(V_1),\ V_4 = \rho_3(V_1). \qquad (5)$$

This is the reason why all vertices have the same distance to p. Hence they are located on a cylinder of revolution with axis p (note the cylinder in Fig. 6). This completes the main arguments for Theorem 1.

According to [4, Remark 2] the flat pose admits a bifurcation between two analytic self-motions of the tessellation mesh. In Fig. 6 poses of both kinds of self-motions are displayed.

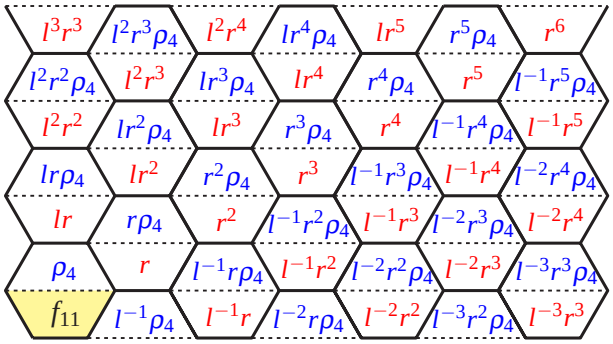

Figure 7: This scheme of a 7×7 tessellation mesh shows the images of f_{11} under the indicated transformations.

Figure 7 shows which transformations must be applied to the face f_{11} to generate all faces of the displayed 7×7 tessellation mesh. If f_{11} and its neighbour face above $f_{21} = \rho_4(f_{11})$ are glued together, then we get a line-symmetric skew hexagon. Its images under products of l and r — as printed in red color — cover the whole mesh.

We note that according to the introduced notation of the faces we have

$$r\colon\ f_{ij} \mapsto f_{i+1\,j+1}, \quad l\colon\ f_{ij} \mapsto f_{i+1\,j-1}.$$

Hence, after applying r^x and l^y on the face f_{11}, we obtain f_{ij} with

$$\begin{pmatrix} i \\ j \end{pmatrix} = \begin{pmatrix} 1 \\ 1 \end{pmatrix} + x\begin{pmatrix} 1 \\ 1 \end{pmatrix} + y\begin{pmatrix} 1 \\ -1 \end{pmatrix} = \begin{pmatrix} 1+x+y \\ 1+x-y \end{pmatrix}$$

with $i+j = 2(1+x) \equiv 0 \pmod 2$. For given i, j with an even sum we can solve these equations for x and y which yields a unique result. For odd $i+j$ at first ρ_4 has to be applied to f_{11}. We summarize:

Lemma 3. *At each nontrivial flexion of an $m\times n$ tessellation mesh the face f_{11} can be transformed into the face f_{ij} according to the following rule:*

$$f_{ij} = \begin{cases} l^{\frac{i-j}{2}} r^{\frac{i+j}{2}-1}(f_{11}) & \text{for } i+j \equiv 0 \pmod 2, \\ l^{\frac{i-j-1}{2}} r^{\frac{i+j-3}{2}} \rho_4(f_{11}) & \text{for } i+j \equiv 1 \pmod 2. \end{cases}$$

Now we focus on the particular case where the quadrangles of the mesh are trapezoids (compare Fig. 10).

Corollary 4. *When the quadrangles of the tessellation mesh are trapezoids, then at each nontrivial flexion either lr or $l^{-1}r$ is a translation along p.*

Proof. According to the proof of Lemma 2 the axis p of the cylinder is the common perpendicular of all axes of half-rotations which exchange pairs of neighbouring faces $(f_{ij}, f_{i+1\,j})$ or $(f_{ij}, f_{i,j+1})$. For each internal edge e_k of a flexion there exists a half-rotation ρ_k mapping e_k onto itself. The axis of ρ_k is orthogonal to e_k (see Fig. 4). There are two cases to distinguish:

- When the axes corresponding to parallel sides e_1, e_2 of any trapezoid of the mesh are not parallel, then their common perpendicular p is unique and necessarily parallel to e_1 and e_2. This means, the folds of one type are aligned; the flexion is trivial in the above-mentioned sense.

- When the axes corresponding to opposite sides of any face f_{ij} are parallel then the product of half-rotations is a translation, which maps one neighbour of f_{ij} onto the neighbour along the opposite side.

The rest can be concluded from Fig. 7. □

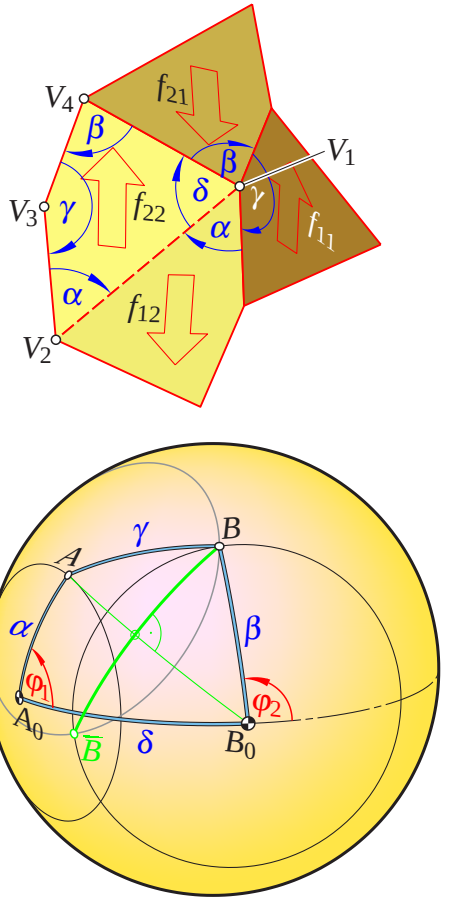

Figure 8: The angles in the flat quadrangle serve as side lengths in the spherical four-bar A_0ABB_0 which controls the dihedral angles of the flexion.

How to compute a flexion? According to Fig. 8 the interior angles of the faces define the side lengths of the *spherical four-bar* which controls all dihedral angles of the flexion. The related formulas can be found in [3, (1)–(6)]. Fig. 8 reveals that for one given bending angle φ_1 there exist two corresponding points B and $\overline{B}$ at the spherical four-bar and therefore two flexions of the tessellation mesh.

There is a second way to compute the flexions: The plane spanned by the convex quadrangle $V_1 \dots V_4$ intersects the cylinder through the vertices (Theorem 1) along an ellipse. There is a pencil of conics passing through $V_1, \dots, V_4$. Hence we can choose any ellipse from this pencil and specify one of the two cylinders of revolution passing through this ellipse. Now we define the half-rotations which generate the flexion: Their axes pass through the midpoints of the sides $V_1V_2, \dots, V_4V_1$ and intersect the cylinder's axis p perpendicularily.

3. CLOSURE CONDITIONS

Can it happen that for a given $m \times n$ tessellation mesh there is a flexion which winds around a cylinder such that the right border line fits exactly to the left border, apart from a vertical shift?

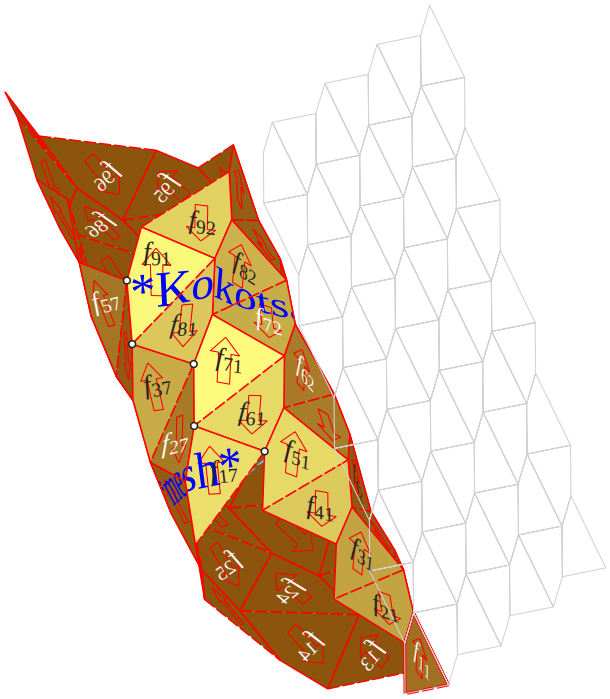

Figure 9: A flexion of a 7×9 tessellation mesh which closes around the cylinder. The flat initial pose is shown in gray color.

Suppose, in a particular flexion which surrounds the cylinder the right border of the face f_{1m} fits exactly to the left border of the mesh. Then we must distinguish two cases:
For *odd* m the face $f_{2m+1} = r(f_{1m})$ is identical with a face of the f_{k1} of the most-left row, $k \equiv 1 \pmod 2$. Lemma 3 implies

$$l^{\frac{1-m}{2}} r^{\frac{m+1}{2}} = l^{\frac{k-1}{2}} r^{\frac{k-1}{2}} d(2\pi)$$

where $d(\pi)$ stands for a rotation about the axis p through 2π. Since the involved helical motions commute pairwise, we obtain

$$r^{\frac{m-k}{2}+1} = l^{\frac{m+k}{2}-1} d(2\pi). \tag{6}$$

We have to note that for each face f_{ij} of the flexion there is a unique helical displacement with $f_{11} \to f_{ij}$. (However, this does not imply that the decompositions according to Lemma 3 are the same.)

For *even* m we obtain in the case of an exact fit that $f_{1\,m+1}$ equals any f_{k1}, $k \equiv 1 \pmod 2$ which means

$$l^{-\frac{m}{2}} r^{\frac{m}{2}} = l^{\frac{k-1}{2}} r^{\frac{k-1}{2}} d(2\pi).$$

This is equivalent to

$$r^{\frac{m-k+1}{2}} = l^{\frac{m+k-1}{2}} d(2\pi). \tag{7}$$

We combine Eqs. (6) and (7) as follows:

Theorem 5. *There is a flexion of the $m \times n$ tessellation mesh where after surrounding the cylinder the right border zig-zag fits exactly to the left border zig-zag if and only if there are two integers $a, b \in \mathbb{Z}$ and*

$$r^a = l^b d(2\pi) \tag{8}$$

where $d(2\pi)$ denotes the full rotation about the cylinder axis p. For odd $m = a+b$ we have $k = b-a+2$, otherwise $k = b-a+1$. A band with $|a-b|$ rows, i.e., an $\infty \times |a-b|$ tessellation mesh with the same quadrangle has a flexion in form of a cylinder tessellation.

4. EXAMPLES

The following two examples fulfilling the closure conditions have been found numerically: The dimensions of the quadrangle and the bending angles have been varied such that after surrounding the cylinder one vertex of the right border line converges against an appropriate vertex of the left border line.

Example 1. At the example depicted in Fig. 9 we have $m = 7$ and $k = 7$ and therefore by (6)

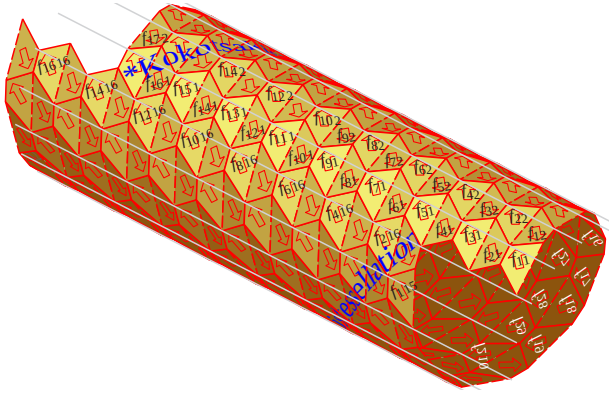

Figure 10: A basic trapezoid yields a modified Schwarz lantern (or Schwarz boot).

$r = l^6 d(2\pi)$, hence $a = 1$ and $b = 6$. The respective angles of rotation and lengths of translation of the related helical displacements are

$$r = (34.614^\circ,\ 21.8738),\ \ l = (-54.231^\circ,\ 3.6456).$$

The basic quadrangle $V_1 \ldots V_4$ has the interior angles 70.0° at V_1, 50.0° at V_2, 160.0° at V_3, and 80.0° at V_4. The side lengths are $V_1V_2 = 25.0$, $V_2V_3 = 13.7416$, $V_3V_4 = 11.7705$, and $V_4V_1 = 17.4653$. The dihedral angles of the depicted flexion are at V_1V_2 205.052° (valley fold), at V_4V_1 145.731°, at V_2V_3 112.759°, and at V_3V_4 143.029°.

The flexion bounds a solid. It can be produced by Boolean operations from the solid cylinder of revolution $\mathscr{C}$ through the vertices as follows: We start with two faces sharing a valley fold (indicated by dashes in the figures). The exterior half spaces of the spans of these two faces intersect in a wedge $\mathscr{W}$. Now we subtract from the solid cylinder $\mathscr{C}$ all wedges which arise from $\mathscr{W}$ by iterated helical displacements r and l.

Example 2. In Fig. 10 the basic quadrangle is an unsymmetric trapezoid. The displayed flexion can be seen as generalized *Schwarz lantern* (or Schwarz boot): The original Schwarz lantern is a triangular mesh approximating a cylindrical surface. The German mathematician Hermann Amandus Schwarz (1843-1921) could prove that depending on the refinement of this mesh the discrete area either converges towards the area

of the cylinder or it tends to infinity.
We notice at the 16×17 tessellation mesh in Fig. 10 that according to Corollary 4 sequences of vertices are placed on generators of the cylinder.

Data: The basic trapezoid has the side lengths $V_1V_2 = 20.0$, $V_2V_3 = 12.9332$, $V_3V_4 = 7.0668$, and $V_4V_1 = 10.9316$. The interior angles at $V_1, \ldots, V_4$ are 65.0°, 50.0°, 130.0° and 115.0°. The bending angle at edge V_1V_2 is 194.6615° (valley fold), at V_2V_3 151.0106°, at V_3V_4 165.3385°, and at V_4V_1 155.5731°. The respective angles of rotation and lengths of translation of the generating helical displacements are

$$r = (22.5^\circ,\ 12.49804),\ \ l = (-22.5^\circ,\ 7.49883).$$

We have $(m,k) = (16,5)$, $(a,b) = (6,10)$ and we can confirm $6 \cdot 12.49804 = 10 \cdot 7.49883$ and $6 \cdot 22.5 = 10 \cdot (-22.5) + 360.0$.

There is an alternative approach to tessellation meshes with a flexion obeying the closing condition: We start with half-turns $\rho_1, \ldots, \rho_4$ such that by (4) the corresponding r and l obey Theorem 5.

First we specify an appropriate cartesian coordinate frame: The x-axis is the axis of the half-turn ρ_1, the z-axis coincides with the helical axis p. Let (r,φ,z) denote the corresponding cylinder coordinates with $x = r\cos\varphi$, $y = r\sin\varphi$.

We set up the respective cylinder coordinates of the axes of ρ_1, ρ_2, ρ_4 by

$$(\mathbb{R}, 0, 0), \quad \left(\mathbb{R}, \frac{\sigma}{2}, \frac{s}{2}\right), \quad \left(\mathbb{R}, \frac{\tau}{2}, \frac{t}{2}\right).$$

Then we obtain in cylinder coordinates according to (1)

$$\begin{aligned}
\rho_1&: (r,\varphi,z) \mapsto (r, -\varphi, -z),\\
\rho_2&: (r,\varphi,z) \mapsto (r, \sigma-\varphi, s-z),\\
\rho_3&: (r,\varphi,z) \mapsto (r, \sigma+\tau-\varphi, s+t-z),\\
\rho_4&: (r,\varphi,z) \mapsto (r, \tau-\varphi, t-z),\\
r&: (r,\varphi,z) \mapsto (r, \sigma+\varphi, s+z),\\
l&: (r,\varphi,z) \mapsto (r, \tau+\varphi, t+z).
\end{aligned}$$

The closure conditions given in Eq. (8) are equivalent to

$$a\sigma = b\tau + 2\pi, \quad as = bt \ \text{ for } \ a,b \in \mathbb{Z}. \qquad (9)$$

By (5) we obtain for any choice of vertex V_1 the other vertices of the face f_{22} (see Fig. 3 or 8). After applying ρ^{-1}, the vertices of f_{11} are

$$\begin{aligned}
V_1 &= (r,\varphi,z),\\
r^{-1}(V_2) &= \rho_1(V_1) = (r,-\varphi,-z),\\
r^{-1}(V_1) &= (r,-\sigma+\varphi,-s+z),\\
r^{-1}(V_4) &= \rho_4(V_1) = (r,\tau-\varphi,t-z).
\end{aligned}$$

However, this implies a condition on V_1: The planarity of this quadrangle is equivalent to

$$\det\begin{pmatrix} 1 & x & y & z\\ 1 & x & -y & -z\\ 1 & x\cos\sigma+y\sin\sigma & y\cos\sigma-x\sin\sigma & z-s\\ 1 & x\cos\tau+y\sin\tau & x\sin\tau-y\cos\tau & t-z \end{pmatrix} = 0.$$

After some computation we obtain from the determinant the polynomial

$$\begin{aligned}
P := {}& [t(\cos\sigma-1)+s(\cos\tau-1)]\,xy\\
&+ (t\sin\sigma+s\sin\tau)\,y^2\\
&+ 2\,[\cos(\sigma+\tau)-\cos\sigma-\cos\tau+1]\,xyz\\
&+ [\sin(\sigma+\tau)-\sin\sigma-\sin\tau]\,(y^2-x^2)z.
\end{aligned} \qquad (10)$$

The zero set of P is a ruled surface of degree 3 with the cylinder axis p (= z-axis) as double line and with generators orthogonal to p. For geometrical reasons this cubic surface passes through the axes of the half-turns $\rho_1, \ldots, \rho_4$.

For a cylinder tessellation with planar quadrangles it is necessary that besides (9) point V_1 is a point of the cubic surface $P = 0$. In addition, we have to check whether the quadrangle is convex. However, for V_1 specified on the axis of ρ_1 we obtain a triangle which of course is convex. Hence a small variation of V_1 gives a planar quadrangle $V_1\ \rho_1(V_1)\ r^{-1}(V_1)\ \rho_4(V_1)$ which is either convex or has a self-intersection. In the latter case we replace V_1 by $\rho_1(V_1)$ in order to obtain convexity. The same holds for V_1 sufficiently close to the axis of ρ_4.

Theorem 6. *For given axes of $\rho_1, \ldots, \rho_4$, each orthogonal to p and obeying (1) and (8), there is a two-parameter set of planar convex quadrangles which are fundamental domains of tessellation meshes with a flexion tiling the cylinder.*

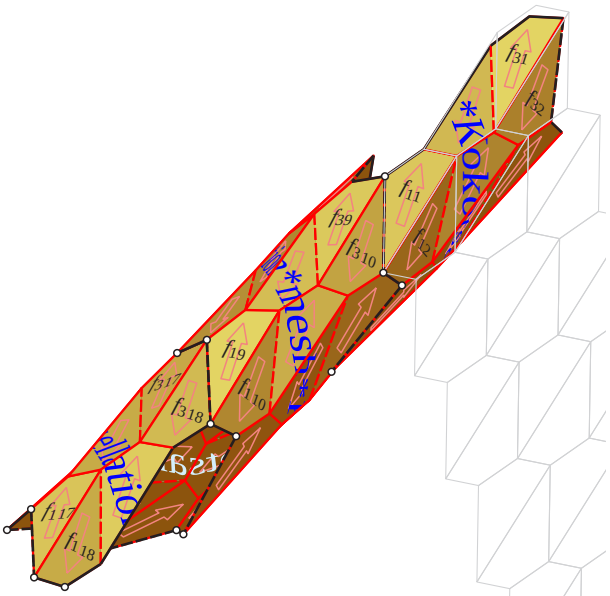

Figure 11: A 18×3 tessellation mesh with a flexion tiling the cylinder (Example 3).

Example 3. Figure 11 shows a flexion of a 18×3 tessellation mesh wrapped without gaps around a cylinder. The base quadrangle $V_1 \dots V_4$ has the interior angles $26.5877°$, $133.6918°$, $132.8933°$, $66.8272°$ and the side lengths $V_1V_2 = 35.0$, $V_2V_3 = 17.2723$, $V_3V_4 = 10.6998$, and $V_4V_1 = 51.7685$. The respective dihedral angles along these edges are $193.2090°$ (valley fold), $133.8661°$, $139.5990°$, and $170.8544°$.
The angles of rotation and lengths of translation of the related helical displacements

$$r = (50.40°,\ 45.30),\ l = (-34.80°,\ 22.65).$$

fulfill (8) with $a = 6$ and $b = 3$.

5. CONCLUSIONS

We studied flexions of the planar tessellation with congruent convex quadrangles. Under the conditions given in Theorem 5 there are flexions which tile a cylinder. This offers a possibility to build rigid discrete models of cylinders of revolution from congruent planar convex quadrangles. One can find the dimensions of such cylinder tiles either numerically by an appropriate algorithm or by starting with a pair of coaxial helical motions r, l obeying Eq. (9) and specifying one vertex on a cubic surface.

ACKNOWLEDGMENTS

This research is supported by Grant No. I 408-N13 of the Austrian Science Fund FWF within the project "Flexible polyhedra and frameworks in different spaces", an international cooperation between FWF and RFBR, the Russian Foundation for Basic Research.

REFERENCES

[1] A. I. Bobenko, T. Hoffmann, and W. K. Schief. On the Integrability of Infinitesimal and Finite Deformations of Polyhedral Surfaces. In A. I. Bobenko et al. (eds.). *Discrete Differential Geometry*. Oberwolfach Seminars 38: 67–93, 2008.

[2] A. Kokotsakis. Über bewegliche Polyeder. *Math. Ann.*, 107: 627–647, 1932.

[3] H. Stachel. A kinematic approach to Kokotsakis meshes. *Comput. Aided Geom. Des.*, 27: 428–437, 2010.

[4] H. Stachel. On the Rigidity of Polygonal Meshes. *South Bohemia Mathematical Letters*, 19(1): 6–17, 2011.

ABOUT THE AUTHOR

Hellmuth Stachel, Ph.D, is Professor emeritus of Geometry at the Institute of Discrete Mathematics and Geometry, Vienna University of Technology, and editor in chief of the "*Journal for Geometry and Graphics*". His research interests are in Higher Geometry and Kinematics. He can be reached by e-mail: stachel@dmg.tuwien.ac.at, by fax: +43-1-58801-10493, or through the postal address: Institute of Discrete Mathematics and Geometry, Vienna University of Technology, Wiedner Hauptstraße 8–10/104, A-1040 Wien, Austria, Europe.